

Reducing the Learning Domain by Using Image Processing to Diagnose COVID-19 from X-Ray Image

Maidar ABAD^{a,1}, Jordi CASAS-ROMA^a and Ferran PRADOS^{a,b,c}

^a*e-Health Center, Universitat Oberta de Catalunya, Barcelona, Spain*

^b*Queen Square MS Centre, Department of Neuroinflammation, UCL Queen Square Institute of Neurology, Faculty of Brain Science, University College of London, London, United Kingdom*

^c*Centre for Medical Image Computing (CMIC), Department of Medical Physics and Bioengineering, University College London, London, UK.*

Abstract. Over the last months, dozens of artificial intelligence (AI) solutions for COVID-19 diagnosis based on chest X-ray image analysis have been proposed. All of them with very impressive sensitivity and specificity results. However, its generalization and translation to the clinical practice are rather challenging due to the discrepancies between domain distributions when training and test data come from different sources. Consequently, applying a trained model on a new data set may have a problem with domain adaptation leading to performance degradation. This research aims to study the impact of image pre-processing on pre-trained deep learning models to reduce the learning domain. The dataset used in this research consists of 5,000 X-ray images obtained from different sources under two categories: negative and positive COVID-19 detection. We implemented transfer learning in 3 popular convolutional neural networks (CNNs), including VGG16, VGG19, and DenseNet169. We repeated the study following the same structure for original and pre-processed images. The pre-processing method is based on the Contrast Limited Adaptive Histogram Equalization (CLAHE) filter application and image registration. After evaluating the models, the CNNs that have been trained with pre-processed images obtained an accuracy score up to 1.2% better than the unprocessed ones. Furthermore, we can observe that in the 3 CNN models, the repeated misclassified images represent 40.9% (207/506) of the original image dataset with the erroneous result. In pre-processed ones, this percentage is 48.9% (249/509). In conclusion, image processing techniques can help to reduce the learning domain for deep learning applications.

Keywords. COVID-19, Transfer Learning, Deep Learning, Medical Image Processing, X-ray Imaging

¹Corresponding Author: Maidar Abad, Universitat Oberta de Catalunya, Rambla del Poblenou, 156, 08018 Barcelona, Spain E-mail: mabdvez@uoc.edu.

1. Introduction

Coronavirus disease 2019 (COVID-19) is a novel illness caused by severe acute respiratory syndrome coronavirus-2 (SARS-CoV-2). According to the World Health Organization, as of May 5th, 2022, there have been about 512M confirmed cases and 6M deaths [1]. Early in the pandemic, expectations were raised that chest CT or chest x-ray (CXR) might play a crucial role in the first-line diagnosis of COVID-19. Over time, the PCR test became more sensitive, and clinicians' understanding of the disease and how to treat it improved. However, the lab test still suffers from insufficient sensitivity, such as 71% reported in Fang et al. [2]. This is due to many factors, such as sample preparation and quality control [3]. Given the current sensitivity of the nucleic acid tests, many suspected patients must be tested multiple times several days apart before reaching a confident diagnosis. Hence, the imaging findings play a critical role in constraining the viral transmission and fighting against COVID-19 [4].

For this reason, over the last 24 months, there have appeared a lot of artificial intelligence (AI) solutions for COVID-19 CXR and CT diagnosis [5]. Compared to the traditional imaging workflow, which relies heavily on human labor, AI enables safer, more accurate, and efficient imaging solutions [4].

To improve diagnosis, Information Technology (IT) services from clinical healthcare institutions have started to install a large number of the possible solutions in their networks, and they have integrated them with their image radiology viewers. In this way, radiologists can select one or more AI algorithms, send the data to compute, and get a diagnostic from each one. However, each of those solutions has been trained with different datasets. This difference in the training data increases the uncertainty of the correctness of any output of any AI solution. This issue is known as domain adaptation [6].

In addition, one of the main problems in evaluating clinical predictions is that deep learning models are often trained and tested on data that do not correspond to the target population and consequently makes it difficult for its generalization and application into a large scale setting. Therefore, a dataset may not adequately represent the range of possible patients and symptoms, generating a bias termed spectrum bias [7]. Because of this bias, most models that obtain high performance may perform poorly in other real-world scenarios where device vendor, acquisition parameters, image quality can vary.

Hence, the end-users of these tools, radiologists, feel overwhelmed with the impressive number of options that they can use from their radiology image viewers and the large number of different answers that they can get depending on the solution they choose.

However, several researchers are still working on developing reliable deep learning tools that can overcome the mentioned shortcomings. Li et al. [8] created a COVID-MobileXpert model for COVID-19 diagnosis on CXR images classified as COVID, Normal, and Pneumonia. They used 429 images for training (149 correspond to COVID-19) and 108 images for testing (36 of COVID-19), obtaining an accuracy of 88%.

Furthermore, Rahaman et al. [9] have compared different transfer learning approaches to identify COVID-19 samples from CXR images. They applied transfer learning to 15 models for 3-class classification (COVID-19, Normal, and Pneumonia). They used 720 images (220 COVID-19) for training and 140 (40 COVID-19) for testing. VGG19 (89.3% accuracy) and VGG16 (88.6% accuracy) showed the best results. Chowdhury et al. [10] trained and validated the ResNet101, MobileNetV2, CheXNet, SqueezeNet, and DenseNet201 models. They used 3,487 CXR images for 2-

class (COVID-19 and Normal) and 3-class classification (COVID-19, Normal, and Pneumonia). DenseNet201 models show the best performance achieving a sensitivity value of 99.7% and 97.9% for COVID-19 detection in the 2-class and 3-class classifications.

Other studies such as the one of Tahir et al. [11] and Rahman et al. [12] have used pre-processing techniques to evaluate the performance of different models. On the one hand, in [11], they have used the Contrast Limited Adaptive Histogram Equalization (CLAHE) filter, lung segmentation and image complement techniques to study its impact on the performance of the SqueezeNet, ResNet18, Inceptionv3, and DenseNet201 models for the classification of images into COVID-19, MERS, and SARS categories. The testing was done on 700 radiographs, of which 423 were COVID-19. The best results were obtained with Inceptionv3 reaching an accuracy of 98% for non-segmented CXR images. On the other hand, in [12], they have explored different image enhancement techniques for segmented and non-segmented CXR images. In this case, the best results were obtained with the ChexNet model and Gamma correlation method achieving an accuracy of 96% for non-segmented images.

In relation to this last study, Heidari et al. [13] have carried out an analysis of the performance of the VGG16 model by applying transfer learning for 3-class (Normal, Pneumonia, and COVID-19) recognition. They have used CXR images by applying diaphragm removal, histogram equalization, and bilateral low-pass filter pre-processing techniques. For the training, they used 8,474 radiographs (415 COVID-19) and 848 images (42 COVID-19) for testing. They obtained a weighted average precision of 95%, a recall of 94%, and an F1-score of 94%. All these studies have shown good performance for the diagnosis of COVID-19 and little generalization possibilities. We can observe that most of the datasets used for training and testing are unstructured, having difficulties over new learning domains for which they have not been trained.

This paper will analyze the impact of some image pre-processing techniques to reduce the learning domain from image-based datasets. For this purpose, we propose a comparison of the performance of unprocessed images and pre-processed images using three different models (VGG16, VGG19, and DenseNet-169) by applying transfer learning. The information in the manuscript is divided as follows: the gathered dataset used is introduced in Section 2.1. The processing techniques and the methodology are described in Sections 2.2 and 2.3, respectively. Section 2.4 presents the metrics used for the performance analysis. The results obtained with the proposed models and discussion are discussed in Section 3. Finally, in Section 4, the conclusions are summarized.

2. Methodology

2.1. Dataset

As a proof of concept, this research used 5,000 posterior anterior (PA) CXR images selected from 6 publicly available datasets to demonstrate the influence of image processing techniques in reducing the learning domain. The selection of the sub-sample taken from the different databases was done randomly. All the images were in PNG format. Of these 5,000 CXR radiographs, 4,000 belonging to the first 4 databases of Table 1 were used for training. 2,000 correspond to COVID-19 positive samples (COVID+), and the remaining 2,000 correspond to Normal or Non-Pathological healthy control (HC) samples. For the test, we used 1,000 images from the last two databases of Table 1.

Table 1. Summary of the datasets used in the research.

DB Name	Data Source	DB Sample Number	Sub-sample Number and Category	Reference
COVID-19 Data Repository	Institute for Diagnostic and Interventional Radiology, Hannover Medical School, Germany	243 COVID+	189 COVID+	[14]
COVID Radiography Dataset	Germany Medical School, SIRM, EURORAD, CXNet, COVID Chest XRay dataset, BIMCV and RSNA	3,616 COVID+ 1,345 Viral Pneumonia 6,012 COVID- Lung Opacity 10,192 HC	1,470 COVID+ 1,099 HC	[15]
COVIDGR	Hospital Universitario Clínico San Cecilio, Granada, Spain	426 COVID+ 426 HC	341 COVID+ 341 HC	[16]
Labeled Optical Coherence Tomography (OCT) and Chest X-Ray Images for Classification	University of California San Diego	4,273 Pneumonia 1,583 HC	560 HC	[17]
Covid ChestXray Dataset	Public sources, hospitals and physicians	506 Viral Pneumonia (468 COVID+) 46 Bacterial Pneumonia 26 Fungal Pneumonia 9 Lipoid Pneumonia 59 Unknown 5,789 Atelectasis 1,010 Cardiomegaly 6,331 Effusion 10,317 Infiltration 6,046 Mass 1,971 Nodule 1,062 Pneumonia 2,793 Pneumothorax 84,312 HC	468 COVID+	[18]
ChestX-ray8	Different hospitals' Picture Archiving and Communication Systems (PACS)		532 HC	[19]

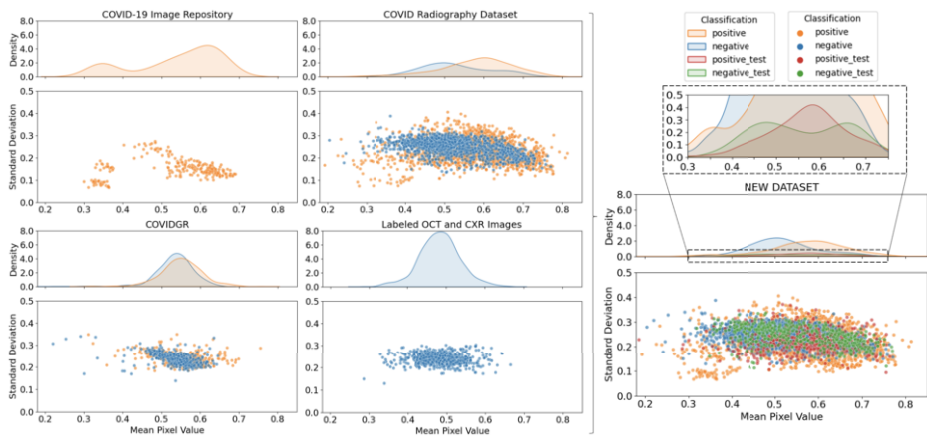


Figure 1. Analysis of the standard deviation and density distribution of the mean pixel value for each image of the datasets used (left) for training to generate the new dataset (right) including the training (in orange and blue) and test images (red and green).

Figure 1 shows the differences between the mean pixel values and the standard deviation of the images in each database and how the new database represents the unification of all the previous ones.

2.2. Data pre-processing

Subsequently, the next step involved pre-processing the incoming images using different techniques to compare the performance of the models with the original or non-preprocessed images and the pre-processed ones. The motivation for the application of pre-processing was, on the one hand, to improve the visual quality of the most damaged area of the lungs by increasing the image contrast through the Contrast Limited Adaptive Histogram Equalization (CLAHE) filter [20]. On the other hand, a rigid registration to an atlas of the lungs was performed for lung alignment and repositioning in the CXR radiographs to fix the deformed images. The atlas was created from the rigid registration

to a half-way space of 1,000 CXR images and the posterior averaging of all of them. Figure 2 shows the comparison between original and processed CXR images.

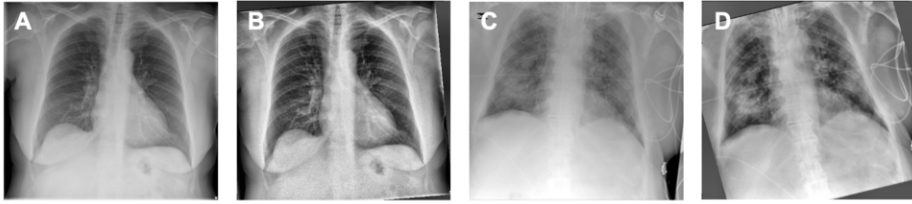


Figure 2. Sample of unprocessed COVID-19 positive case (A), unprocessed COVID-19 negative case (C) and their result after applying CLAHE filter and image registration (B,D).

2.3. Proposed method

Training models for disease detection requires a large data size, which sometimes may be difficult to achieve. To overcome the limited data size, we took advantage of pre-trained deep neural networks and transfer learning approaches. Pre-trained neural networks allow us to use a large number of parameters that have been previously trained on other datasets. Those parameters can be easily adapted to a new task with few modifications. Transfer learning is particularly beneficial in cases where there are not enough training samples to train a model from scratch, as may be the case for COVID-19 images.

We used transfer learning through ImageNet data which contains millions of labeled images. We applied this method to VGG16, VGG19 and DenseNet169 pre-trained deep neural networks to classify CXR images into negative and positive COVID-19 classes.

In addition, all images in the dataset were normalized between 0 and 1 and resized to 480 x 480 pixels. In the case of using the unprocessed database, no further modifications were applied to the images. In the case of the preprocessed images, we realigned all the images to an in-house lung atlas template using a rigid transformation and afterwards applied a CLAHE filter [20] to automatically enhance the contrast of each image.

We took the architectures of the trained CNNs with ImageNet, which includes 1,000 class lists, for transfer learning [21]. The set of features learned by these networks was used by transfer learning to extract specific features related to COVID-19 detection. The weights of each layer of the CNN models were frozen, except for those of the fully connected output layer. This layer was removed to adapt the model to the new classification problem. The default hyperparameters for each of the networks were maintained.

We added six layers on the top of each model (Figure 3). First, we set a 4x4 Average Pooling layer to take the average value of the features from the feature maps, and thus reduce computation complexity and variance avoiding overfitting. Next, we added a Flatten layer to convert the multi-dimensional data into 1-dimensional array. Then, we attached two fully connected layers with an output of 128 and 64, respectively, using Rectified Linear Unit (ReLU) activation function. ReLU, which is defined as: $\text{ReLU}(x) = \max(0, x)$, is applied after each of those layer to make the network non-linear. We also add a dropout layer with a rate of 0.5 to avoid overfitting. Finally, another fully connected layer with a softmax classifier and an output of two classes corresponding to negative and positive COVID-19 detection. Softmax assigns each node a number between 0 and

1, being the sum of all probabilities equal to 1. To train the CNN models, we set the batch size to 10 and the number of epochs to 20. We used the Adam optimizer with a learning rate of 0.0001 for optimization. Adam optimization is a stochastic gradient descent method that involves a combination of first and second-order moments. In this work, we employed categorical cross-entropy as the loss function. Moreover, we used early stopping as a kind of regularization used to avoid overfitting when training. The criterion we have used is based on stopping training when the validation loss increases noticeably.



Figure 3. Transfer learning model scheme.

The training dataset (databases 1-4 of Table 1) was split using 10% of the images for validation and 90% for training. In addition, the partition was 50% COVID+ and 50% HC and all datasets were included in the training and validation groups. Test has been done with an independent dataset (databases 5-6 of Table 1) that has not been used for training. The partitioning of the testing dataset is 46.8% COVID+ and 53.2% HC.

2.4. Performance analysis

We evaluated true positives (TP) and true negatives (TN) to represent images that were well classified as COVID+ or HC respectively, while false positives (FP) and false negatives (FN) represent the misclassified images. The performance was measured in terms of sensitivity, specificity, accuracy, F1-score, and precision.

3. Results and Discussion

By testing the unprocessed and pre-processed images and applying the metrics mentioned in the performance analysis, we obtained the results shown in Table 2. We observe an improvement in accuracy (+1.1%) for the pre-processed images (82.5%) compared to the unprocessed ones (81.4%) for VGG16 model. In addition, we see that the sensitivity improves notoriously (+4.8%) for VGG16 model. This value is crucial for COVID-19 detection as it indicates a decrease in FN values (see Figure 4). As for the specificity, we observe that the value decreases (by -2.6%) in the pre-processed images because of the slight increase in the FN values, as shown in the confusion matrices (Figure 4). Moreover, for this reason, the precision value is reduced by 1.0% in the pre-processed images, and the F1-score improves by 1.7%.

The VGG19 model testing results do not show the same pattern as in the previous model presented in Table 2 and Figure 4. In this case, the accuracy of the pre-processed images decreases up to 82.6% (by -0.6%) as an F1-score 82.2% (by -1.0%), and sensitiv-

Table 2. Comparison between unprocessed and processed images for the three networks in terms of accuracy, precision, sensitivity, specificity and F1-score (%). The best results are shown in bold. All the metrics results are reported considering the 95% confidence interval.

CNN Model	Dataset	Accuracy	Specificity	Sensitivity	F1-score	Precision
VGG16	Original	81.4 ± 2.4 CI[79.0 to 83.8]	79.4 ± 3.4 CI[76.0 to 82.8]	83.4 ± 3.4 CI[80.0 to 86.8]	81.7 ± 3.5 CI[78.2 to 85.2]	80.2 ± 3.6 CI[76.6 to 83.8]
	Pre-processed	82.5 ± 2.4 CI[80.1 to 84.9]	76.8 ± 3.6 CI[73.2 to 80.4]	88.2 ± 2.9 CI[85.3 to 91.1]	83.4 ± 3.4 CI[80.0 to 86.8]	79.2 ± 3.7 CI[75.5 to 82.9]
VGG19	Original	83.2 ± 2.3 CI[80.9 to 85.5]	83.0 ± 3.2 CI[79.8 to 86.2]	83.4 ± 3.4 CI[80.0 to 86.8]	83.2 ± 3.4 CI[79.8 to 86.6]	83.1 ± 3.4 CI[79.7 to 86.5]
	Pre-processed	82.6 ± 2.3 CI[80.3 to 84.9]	85.0 ± 3.0 CI[82.0 to 88.0]	80.2 ± 3.6 CI[76.6 to 83.8]	82.2 ± 3.5 CI[78.7 to 85.7]	84.2 ± 3.3 CI[80.9 to 87.5]
DenseNet-169	Original	82.8 ± 2.3 CI[80.5 to 85.1]	82.0 ± 3.3 CI[78.7 to 85.3]	83.6 ± 3.4 CI[80.2 to 87.0]	82.9 ± 3.4 CI[79.5 to 86.3]	82.3 ± 3.5 CI[78.8 to 85.8]
	Pre-processed	84.0 ± 2.3 CI[81.7 to 86.3]	77.6 ± 3.5 CI[74.1 to 81.1]	90.4 ± 2.7 CI[87.7 to 93.1]	85.0 ± 3.2 CI[81.8 to 88.2]	80.1 ± 3.6 CI[76.5 to 83.7]

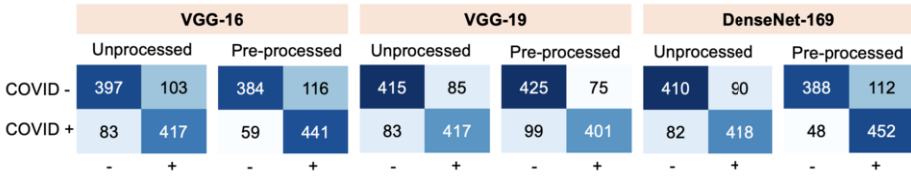


Figure 4. The figure shows the confusion matrix results after testing the three models. Positive cases are indicated as COVID+ or “+”, and negative cases as COVID- or “-”. Rows represent the true label and columns represent the predicted label.

ity to 66.2% (by -3.2%). However, specificity increases by 2.0% and precision by 1.1%. This is related to the results of the confusion matrices in Figure 4.

Regarding the test results for DenseNet-169 model (Table 2), we see an increase in accuracy from 82.8% to 84.0% for the pre-processed images. Similarly, the F1-score increases to 85.0% for the pre-processed images and the sensitivity to 90.4%. In this case, specificity decreases by 4.8% and precision by 2.2%. In this case, the confusion matrices of Figure 4 show a notorious reduction of 41.5% in the FN values of the pre-processed images. Consequently, there is a 24.4% increase in the FP values.

Overall, the best results have been obtained for the pre-processed images, which is related to the accuracy and sensitivity increase. This last point is remarkable since it indicates that the number of images classified as FN, which represent COVID+ cases classified as HC, is reduced.

In addition, we performed a study to compare the images classified as FN and FP considering the three models (VGG16, VGG19, and DenseNet-169) for the two datasets (original and preprocessed). We found that the repeated misclassified images represent 40.9% of the original image dataset with the erroneous result since 207 repeated images (69 images for each CNN model) were present in a total of 506 misclassified unprocessed images for the three models. This percentage is 48.9% in pre-processed ones since 249 repeated images (83 images for each CNN model) were present in a total of 509 misclassified pre-processed images.

Considering that a large part of the misclassified images are repeated, we wanted to check if there is a pattern capable of differentiating these images from those that have been well classified (TN and TP) by the three models in each dataset. To do this, we first studied the mean pixel values and the standard deviation of each group. Figure 5 shows that the mean pixel values of the TN images are clustered between 0.40 and 0.75 on a scale of 0 to 1. While the TP images extend equally over a wide range in the case of the unprocessed images, the pre-processed images show a density peak between 0.50 and 0.65 values. FN and FP values are under the spectrum of the well classified, so it is hard to draw a clear differentiation.

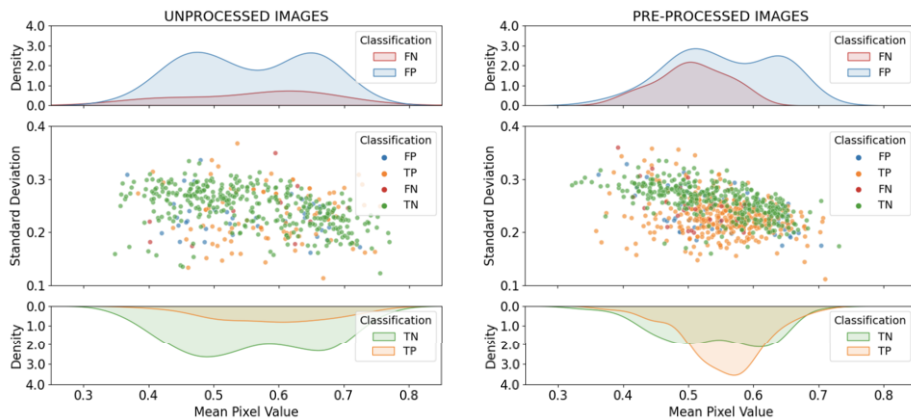


Figure 5. Representation of the standard deviation and density of the mean pixel values for each image classified as TP, TN, FP and FN.

With the purpose of looking for differentiation between misclassified and well-classified images, we carried out an entropy's study to compare both groups. Within this study, we have considered as FN and FP only images equally misclassified by the three models. The groups TP and TN correspond to the images equally well classified as TP or TN by the three models. Shannon Entropy [22] is a measure from information theory which represents the level of uncertainty of a set of values and we employed it to characterize the overall image's texture coherence.

Figure 6 shows the results of this study, where we can observe a clear differentiation between the misclassified images, which have higher entropy values, and the well-classified ones. This difference could serve as an initial filter for identifying these images before using them in convolutional networks.

Furthermore, we studied contrast, signal-to-noise ratio (SNR) and image normalized entropy parameters to detect similarities between misclassified and well-classified images. To this end, after calculating those parameters for each image, we applied the t-test to check whether the groups were statistically different or not. The significance level has been set to $p < 0.05$. Table 3 shows the results of the different p-values obtained in the tests considering as FN and FP the images misclassified in common by the three models at each dataset, and TP and TN as the well classified images in common by the three models at each dataset. The results indicate that FN images are misclassified because their resemblance to the TN images in terms of SNR and contrast.

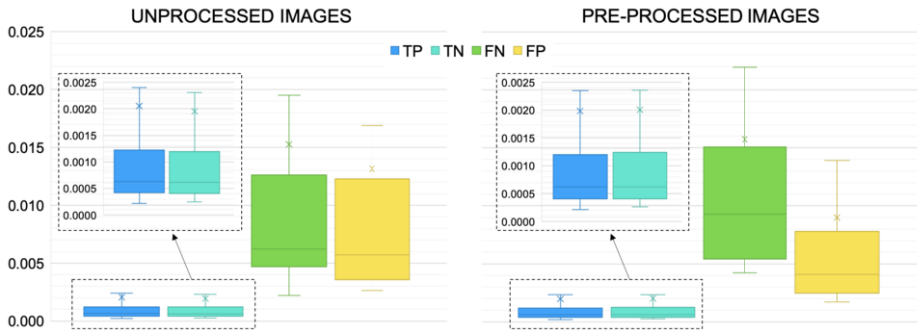


Figure 6. Representation of the Shannon entropy for each image classified as TP, TN, FP and FN.

Table 3. Results of the p-values obtained from the t-test.

Metric	Dataset	FN-TN	FN-TP	FP-TN	FP-TP
SNR	Original	0.865	<0.001	0.215	0.004
	Pre-processed	0.464	<0.001	0.002	0.447
Contrast	Original	0.954	<0.001	<0.001	0.017
	Pre-processed	0.286	<0.001	0.690	<0.001
Entropy	Original	0.006	0.006	0.005	0.005
	Pre-processed	0.004	0.004	0.003	0.002

4. Conclusion

In the present work, we conducted a comparative study of three CNN models trained and tested with unprocessed and pre-processed CXR images to detect COVID-19. For this purpose, we have created a dataset using 5,000 images from various publicly available sources. After evaluating different classic metrics such as accuracy, sensitivity, or specificity, we have found that in most cases accuracy and sensitivity improve when using pre-processed images. We found that these pre-processing steps are directly related to the decrease of images wrongly classified as non-COVID-19. The CNN model DenseNet-169, trained and tested on pre-processed images, achieved an accuracy of 84.0%, a sensitivity of 90.4%, and a specificity of 77.6%, showing the best performance results in terms of positive COVID-19 detection. In addition, we have demonstrated that many misclassified images show higher entropy values than the well-classified ones, so our future work will focus on introducing an entropy filter for improving the performance of the prediction models. Moreover, we would like to implement other processing techniques such as those in [11,12,13] and thus test the change in learning domain reduction in both the models used in this article and in others mentioned in [11,12,9]. In conclusion, this study has shown that well selected image processing techniques can help to reduce the learning domain for deep learning applications.

References

[1] WHO Coronavirus (COVID-19) Dashboard;. Accessed: 2022-5-9. <https://covid19.who.int>.

- [2] Fang Y, Zhang H, Xie J, Lin M, Ying L, Pang P, et al.. Sensitivity of Chest CT for COVID-19: Comparison to RT-PCR; 2020.
- [3] Rahmani AM, Mirmahaleh SYH. Coronavirus disease (COVID-19) prevention and treatment methods and effective parameters: A systematic literature review. *Sustain Cities Soc.* 2021 Jan;64:102568.
- [4] Shi F, Wang J, Shi J, Wu Z, Wang Q, Tang Z, et al. Review of Artificial Intelligence Techniques in Imaging Data Acquisition, Segmentation, and Diagnosis for COVID-19. *IEEE Rev Biomed Eng.* 2021 Jan;14:4-15.
- [5] Bullock J, Luccioni A, Pham KH, Lam CSN, Luengo-Oroz M. Mapping the landscape of Artificial Intelligence applications against COVID-19; 2020.
- [6] Choudhary A, Tong L, Zhu Y, Wang MD. Advancing Medical Imaging Informatics by Deep Learning-Based Domain Adaptation. *Yearb Med Inform.* 2020 Aug;29(1):129-38.
- [7] Varoquaux G, Cheplygina V. Machine learning for medical imaging: methodological failures and recommendations for the future. *NPJ Digit Med.* 2022 Apr;5(1):48.
- [8] Li X, Li C, Zhu D. COVID-MobileXpert: On-Device COVID-19 Patient Triage and Follow-up using Chest X-rays; 2020.
- [9] Rahaman MM, Li C, Yao Y, Kulwa F, Rahman MA, Wang Q, et al. Identification of COVID-19 samples from chest X-Ray images using deep learning: A comparison of transfer learning approaches. *J Xray Sci Technol.* 2020;28(5):821-39.
- [10] Chowdhury MEH, Rahman T, Khandakar A, Mazhar R, Kadir MA, Mahub ZB, et al.. Can AI Help in Screening Viral and COVID-19 Pneumonia?; 2020.
- [11] Tahir AM, Qiblawey Y, Khandakar A, Rahman T, Khurshid U, Musharavati F, et al. Deep Learning for Reliable Classification of COVID-19, MERS, and SARS from Chest X-ray Images. *Cognit Comput.* 2022 Jan:1-21.
- [12] Rahman T, Khandakar A, Qiblawey Y, Tahir A, Kiranyaz S, Kashem SBA, et al.. Exploring the effect of image enhancement techniques on COVID-19 detection using chest X-ray images; 2021.
- [13] Heidari M, Mirniaharikandehi S, Khuzani AZ, Danala G, Qiu Y, Zheng B. Improving the performance of CNN to predict the likelihood of COVID-19 using chest X-ray images with preprocessing algorithms; 2020.
- [14] ml-workgroup. GitHub - ml-workgroup/covid-19-image-repository: Anonymized dataset of COVID-19 cases with a focus on radiological imaging. This includes images (x-ray / ct) with extensive meta-data, such as admission-, ICU-, laboratory-, and patient master-data;. Accessed: 2022-5-9. <https://github.com/ml-workgroup/covid-19-image-repository>.
- [15] Rahman T. COVID-19 Radiography Database;.
- [16] Tabik S, Gomez-Rios A, Martin-Rodriguez JL, Sevillano-Garcia I, Rey-Area M, Charte D, et al. COVIDGR Dataset and COVID-SDNet Methodology for Predicting COVID-19 Based on Chest X-Ray Images. *IEEE J Biomed Health Inform.* 2020 Dec;24(12):3595-605.
- [17] Kermany D. Labeled Optical Coherence Tomography (OCT) and Chest X-Ray Images for Classification. *Mendeley Data*; 2018.
- [18] iieee8023. IEEE8023/covid-chestxray-dataset: We are building an open database of COVID-19 cases with chest X-ray or CT images;. Available from: <https://github.com/ieee8023/covid-chestxray-dataset>.
- [19] Wang X, Peng Y, Lu L, Lu Z, Bagheri M, Summers RM. ChestX-ray8: Hospital-Scale Chest X-Ray Database and Benchmarks on Weakly-Supervised Classification and Localization of Common Thorax Diseases. *Proceedings of the IEEE Conference on Computer Vision and Pattern Recognition (CVPR).* 2017 July.
- [20] Asnaoui KE, El Asnaoui K, Chawki Y, Idri A. Automated Methods for Detection and Classification Pneumonia Based on X-Ray Images Using Deep Learning; 2021.
- [21] Deng J, Dong W, Socher R, Li LJ, Li K, Fei-Fei L. ImageNet: A large-scale hierarchical image database; 2009.
- [22] Shannon CE. A mathematical theory of communication. *The Bell System Technical Journal.* 1948;27(3):379-423.